

MODEL PREDICTIVE CONTROL OF HYDROGEN–ELECTRIC AIRPORT ENERGY SYSTEMS FOR SUSTAINABLE GROUND OPERATIONS

Yuanzhe Chen[1]

[1]School of Electrical Engineering and Telecommunications, University of New South Wales (UNSW Sydney), Sydney NSW 2052, Australia

Abstract

Airport ground support equipment (GSE) electrification creates large, schedule-driven charging loads that challenge depot energy management. Prior work addresses battery-electric vehicle (BEV) charging and hydrogen fuel-cell vehicle (FCEV) electrolyser dispatch as separate optimisation layers, leaving shared photovoltaic (PV) resources suboptimally allocated. This paper proposes a model predictive controller (MPC) that dispatches BEV charging, FCEV electrolyser operation, and grid import in a single 41-variable convex quadratic program (QP) per step. Per-vehicle lower bounds derived from flight-schedule departure deadlines enforce mission-readiness without over-charging. The QP is solved by an analytical gradient-projection algorithm requiring no external solver, achieving a mean step time of 0.14 ms — 370 times faster than a 50 ms embedded deployment limit. Full-year simulation on publicly available NREL eGSE 8760-hour load data (Austin-Bergstrom Airport, 50% electrification) and NSRDB solar irradiance data demonstrates a 28.2% reduction in annual peak grid demand relative to an uncoordinated greedy baseline, stable BEV fleet SOC maintained near the 0.90 mission-ready threshold, and 221 kg H_2 produced annually from solar surplus.

Keywords: model predictive control, airport ground support equipment, hydrogen electrolysis, BEV fleet charging, peak shaving

1. Introduction

Aviation faces acute decarbonisation pressure. Raihan [1] provides a comprehensive review of sustainable aviation policy, noting that while meaningful progress has been achieved in sustainable aviation fuel (SAF) development and emissions optimisation, the sector faces substantial hurdles in aligning with global climate goals; the review identifies integrated policy approaches and investment in renewable propulsion — including electric and hydrogen technologies — as critical enablers. At the strategic level, Canturk [2] shows that energy management has moved to the centre of decision-making in airports and airlines, arguing that electrification and renewable energy integration create value not only by reducing emissions but also by improving cost stability and operational resilience. The World Economic Forum's Airports of Tomorrow initiative [3] reinforces this direction, seeking to overhaul global airports into clean energy hubs by mobilising capital for hydrogen and battery-electric technologies.

A practical pathway to airport decarbonisation is the replacement of diesel GSE fleets with BEVs and FCEVs. Kemperdick and Letmathe [4] compare the external costs of BEV and FCEV powertrains for heavy-duty applications using a Well-to-Wheel analysis, finding that BEVs cause the least external costs in most cases but that energy source and payload significantly affect outcomes — motivating mixed BEV/FCEV fleet deployments in airport contexts where both fast charging and rapid hydrogen refuelling are required. Guo et al. [5] develop a bi-objective infrastructure planning framework

for airport microgrids integrating electric aircraft and parking-lot EVs, demonstrating that V2G strategies improve microgrid economic performance while plug-in charging outperforms battery-swap in resilience.

At the system level, Xiang et al. [6] propose a hydrogen-solar-storage integrated microgrid for airport electrification and show — via mixed-integer linear programming optimisation — that integrating hydrogen energy systems reduces total annual costs and carbon emissions by **41.6%** and **67.29%** respectively compared to benchmark scenarios. Goh et al. [7] develop an adaptive MPC energy management strategy for Copenhagen Airport using wind, PV, and waste-to-energy sources, confirming feasibility for achieving carbon neutrality by 2050; their simulations show renewable generation covering 81% of airport electricity demand in summer at a daily operating cost of USD 36,087.83. Canturk [2] further notes that airports integrating renewable energy and electrification gain competitive advantage through cost stability and reduced exposure to fossil fuel price volatility.

MPC has become the dominant paradigm for real-time EV fleet energy management in grid-connected microgrids. Hermans et al. [8] implement an MPC controller for a fleet of 174 EV chargers co-located with PV generation at a corporate microgrid in the Netherlands, formulating the problem as a QP solved by open-source Python libraries; their three-week deployment achieves an average daily grid peak reduction of **59%**. Minchala-Ávila et al. [9] conduct a systematic review of 101 MPC studies for EV integration and V2G applications (PRISMA 2020), finding that predictive control strategies achieve up to 35% reduction in frequency deviations, 20–30% mitigation of harmonic distortion, and 15–20% extension of battery lifespan, while identifying *high computational demands*, limited scalability, and the absence of standardised communication frameworks as major barriers to large-scale deployment. Sadiq et al. [10] apply decentralised MPC to an offshore wind-powered seaport DC microgrid with EV charging stations, demonstrating that MPC preserves MVDC bus voltage stability while optimising power flow and minimising energy losses under stochastic EV arrival patterns.

Several studies address the joint scheduling of EVs and electrolysers. Zhang et al. [11] formulate an MPC-based co-optimisation of a PV–EV–hydrogen fuelling station, using second-order cone programming to handle AC power-flow nonlinearities; results on a modified IEEE 33-bus system show a **12%** reduction in transmission loss and a **53%** improvement in EV user comfort. Massana et al. [12] propose a genetic-algorithm-based multi-vector energy management system for a Spanish technology park (360 kW peak consumption) that jointly schedules an electrolyser, EV charging station, hydrogen refuelling station, and HVAC; real-time experiments over 14 days confirm that the scheduler maximises local renewable utilisation by shifting demand to surplus-generation hours. García-Triviño et al. [13] design a supervisory control system for a grid-connected MVDC microgrid combining PV, battery, green hydrogen (fuel cell and electrolyser), and EV fast chargers; hardware-in-the-loop tests confirm proper operation and economic benefit from grid energy sales. Elmasry et al. [14] study an electricity–hydrogen nexus with multi-level hydrogen storage (30, 350, and 700 bar) serving BEV, FCEV car, and FCEV truck charging points; their cost-optimised solution produces the most hydrogen *during nighttime when electricity is inexpensive*, at a daily energy cost of $1045.65.

A critical challenge for embedded MPC deployment is computational tractability. Babojelić et al. [15] propose a set-based fast gradient projection algorithm for MPC of grid-tied power converters, implemented on TI DSP and Xilinx FPGA platforms; their hardware-in-the-loop results demonstrate that gradient-projection MPC satisfies the strict timing constraints of fast power converter dynamics without relying on external optimisation libraries.

A gap persists in the literature: existing airport microgrid controllers either focus on *static capacity sizing* [6, 5] or treat BEV charging and electrolyser dispatch as *sequential layers* [12, 13], and those that use real-time MPC for EV fleets [8, 11] rely on external QP solvers that preclude sub-millisecond embedded deployment [9]. No prior work simultaneously: (i) couples BEV and FCEV electrolyser dispatch in a single QP for an airport GSE depot; (ii) enforces mission-departure SOC deadlines arising from flight schedules; and (iii) solves the QP without any external solver at sub-millisecond speed.

This paper makes four contributions:

1. **Single-QP coupled controller.** BEV charging ($N_{\mathrm{BEV}} = 20$), FCEV electrolyser ($N_{\mathrm{FCEV}} = 20$), and hydrogen electrolyser (p_{el}) are jointly optimised in one 41-variable convex QP per step,

eliminating suboptimality from sequential layering.

2. **Mission-deadline SOC constraints.** Per-vehicle charging lower bounds are derived from flight-schedule departure deadlines, ensuring vehicles reach SOC ≥ 0.90 before each mission.

3. **Solver-free gradient projection.** Following the framework of [15], the QP is solved by projected gradient descent with $O(N)$ per-step complexity; mean solve time is 0.14 ms (max 1.44 ms), satisfying the 50 ms embedded limit by a factor of 370.

4. **Full-year simulation.** Validated on NREL eGSE 8760-hour load profiles and NSRDB solar irradiance data; 28.2% peak demand reduction and 221 kg H_2/year production demonstrated.

2. System Model

2.1 Depot Microgrid Architecture

The airport GSE depot microgrid comprises: a 500 kWp rooftop PV array; a charger bank ($P_{\text{ch,max}} = 800$ kW) serving $N_{\text{BEV}} = 20$ BEVs ($E_{\text{BEV}} = 90$ kWh each); a PEM electrolyser ($P_{\text{el,max}} = 500$ kW, $\eta_{\text{el}} = 0.70$) producing H_2 for $N_{\text{FCEV}} = 20$ FCEVs ($E_{\text{FCEV}} = 45$ kWh equivalent); and a constant depot baseload $P_{\text{base}} = 300$ kW. This architecture follows the hydrogen-solar-storage airport microgrid concept of Xiang et al. [6], extended to include a mixed BEV/FCEV GSE fleet as motivated by [4].
The instantaneous grid import is:

$$P_{\text{grid}}(t) = P_{\text{base}} + \sum_i u_{\text{bev},i}(t) + \sum_j u_{\text{fcev},j}(t) + p_{\text{el}}(t) - P_{\text{pv}}(t). \tag{1}$$

2.2 Vehicle SOC Dynamics

BEV state-of-charge (SOC) evolves as:

$$\text{SOC}_i(t+1) = \begin{cases} \text{SOC}_i(t) + \dfrac{\eta_c\, u_{\text{bev},i}}{E_{\text{BEV}}}, & a_i(t) = 1, \\ \max(\text{SOC}_{\min},\, \text{SOC}_i(t) - \delta), & a_i(t) = 0, \end{cases} \tag{2}$$

where $a_i(t) \in \{0,1\}$ is the depot-availability flag, $\eta_c = 0.92$, $\text{SOC}_{\min} = 0.20$, and $\delta = 0.055$ is the fractional energy consumed per mission-hour. FCEV dynamics are analogous with E_{FCEV} and η_{el}.

2.3 Mission Availability and Departure Deadlines

Vehicle availability is sampled from the NREL eGSE hourly load profile (Austin-Bergstrom Airport, 50% electrification, 8760-hour dataset):

$$\Pr[a_i(t) = 1] = 1 - \frac{D(t)}{D_{\max}}, \tag{3}$$

where $D(t)$ is fleet-level demand and $D_{\max}$ is its annual maximum. Each vehicle's departure deadline $d_i(t)$ is computed offline as the number of hours until its next on-mission transition. This schedule-aware approach follows the observation of Goh et al. [7] that airport operational characteristics must be embedded in energy management strategies to achieve practical feasibility.

2.4 PV Generation Model

AC PV output is:

$$P_{\text{pv}}(t) = \frac{G(t)}{G_{\text{STC}}} \cdot P_{\text{pv,rated}} \cdot \text{PR}, \tag{4}$$

where $G(t)$ is GHI from the NSRDB one-axis dataset (Sydney Airport proxy, $-33.86°$, $151.21°$, UTC, 2019), $G_{\text{STC}} = 1000$ W/m^2, $P_{\text{pv,rated}} = 500$ kWp, and $\text{PR} = 0.80$.

3. MPC Formulation and Solver

3.1 Decision Variables

At each hourly step t the controller determines:

$$\mathbf{u}(t) = \left[u_{\text{bev},1}, \ldots, u_{\text{bev},20},\ u_{\text{fcev},1}, \ldots, u_{\text{fcev},20},\ p_{\text{el}}\right]^\top \in \mathbb{R}^{41}, \tag{5}$$

comprising 20 BEV charging powers, 20 FCEV electrolyser powers, and the central hydrogen electrolyser dispatch.

3.2 Coupled Convex QP Objective

$$\begin{aligned}\min_{\mathbf{u}} J = {} & W_p \left(P_{\text{grid}} - P_{\text{cap}}\right)_+^2 + W_c\, c(t)\, P_{\text{grid}} \\ & - W_e\, p_{\text{el}}\, \mathbf{1}[P_{\text{pv}} > P_{\text{base}}] + W_s \|\mathbf{u} - \mathbf{u}_{\text{prev}}\|^2 \\ & - \alpha(t)^\top \mathbf{u},\end{aligned} \tag{6}$$

where $(\cdot)_+ = \max(\cdot, 0)$ is the one-sided peak penalty; $P_{\text{cap}} = 600$ kW; $c(t)$ is the time-of-use electricity price; $W_p = 3.0$, $W_c = 2.0$, $W_e = 1.5$, $W_s = 0.04$; and α is a per-vehicle urgency vector:

$$\alpha_i(t) = W_u \frac{(\text{SOC}_{\text{dep}} - \text{SOC}_i(t))^+}{\max(d_i(t), 1)}, \quad W_u = 2.5, \tag{7}$$

active when $d_i < 8$ and $\text{SOC}_i < 0.90$. The five terms respectively penalise grid peak excess, energy cost, reward PV-surplus electrolyser dispatch, penalise control variation, and incentivise urgent charging. This couples mission-deadline awareness directly into the shared QP, an extension absent in prior coupled schedulers [12, 11].

3.3 Constraints

The optimisation is subject to:

$$\ell_i(t) \le u_{\text{bev},i} \le \bar{u}_i(t), \quad \forall i, \tag{8}$$

$$0 \le p_{\text{el}} \le \min\left(P_{\text{el,max}}, \max(0, P_{\text{pv}} - P_{\text{base}})\right), \tag{9}$$

$$\sum_i u_{\text{bev},i} + \sum_j u_{\text{fcev},j} \le P_{\text{ch,max}}, \tag{10}$$

where $\ell_i = \min(E_{\text{need},i}/(\eta_c\, d_i), \bar{u}_i)$, $E_{\text{need},i} = (\text{SOC}_{\text{dep}} - \text{SOC}_i)^+ E_{\text{BEV}}$, is the minimum charging input rate to reach $\text{SOC}_{\text{dep}} = 0.90$ in time, and $\bar{u}_i = \min(P_{\text{bev,max}}, (1 - \text{SOC}_i) E_{\text{BEV}}/(\eta_c \Delta t))$ is the SOC-headroom ceiling. Constraint (9) restricts the electrolyser to absorb only PV surplus above P_{base}, consistent with the nighttime/low-price electrolyser strategy identified by Elmasry et al. [14] and ensuring the electrolyser never increases net grid draw. Constraint (10) enforces the shared charger bank capacity.

3.4 Gradient-Projection Solver

Because objective (6) is convex and quadratic, and constraints (8)–(10) define a box plus a single affine coupling constraint, the QP is solved by projected gradient descent (PGD):

$$\mathbf{u}^{(k+1)} = \Pi_{\mathscr{C}}\left(\mathbf{u}^{(k)} - \mu\, \nabla J\right), \quad \mu = 0.20, \tag{11}$$

where $\Pi_{\mathscr{C}}$ projects onto the feasible set $\mathscr{C}$ via box clipping ($O(N)$) followed by a proportional scaling for the charger-bank constraint ($O(N)$). This approach extends the set-based fast gradient projection framework of Babojelić et al. [15] from single-converter MPC to a multi-asset fleet scheduling context. The total per-step complexity is $O(N \cdot K_{\max})$ with $K_{\max} = 100$ and a warm start from $\mathbf{u}_{\text{prev}}$; convergence typically occurs within 20–40 iterations.

The gradient of objective (6) with respect to $\mathbf{u}$ is:

$$\nabla J = \left[2W_p(P_{\text{grid}} - P_{\text{cap}})_+ + W_c\, c(t)\right]\mathbf{1} + 2W_s(\mathbf{u} - \mathbf{u}_{\text{prev}}) - \alpha - W_e\, \mathbf{1}[P_{\text{pv}} > P_{\text{base}}]\, \mathbf{e}_{41}, \tag{12}$$

where $\mathbf{e}_{41}$ is the unit vector selecting the electrolyser component. Since $P_{\text{grid}} = P_{\text{base}} + \mathbf{1}^\top \mathbf{u} - P_{\text{pv}}$ is linear in $\mathbf{u}$, the gradient is computable in $O(N)$ per step, confirming the overall $O(N \cdot K)$ solver complexity.

4. Simulation Setup

4.1 Datasets

eGSE load. Hourly BEV/FCEV charging demand profiles are from the NREL eGSE 8760-hour dataset (Austin-Bergstrom International Airport, 50% electrification scenario; data available at `data.nrel.gov/submissions/279`). The dataset provides flight-schedule-driven demand patterns for each hour of the year, enabling realistic mission availability modelling.

Solar irradiance. One-axis tracking GHI data are from the NSRDB ($-33.86°$, $151.21°$, UTC, 2019; `nsrdb.nrel.gov`), serving as a Sydney Airport proxy consistent with the Southern Hemisphere airport microgrid context of this study.

Electricity price. The time-of-use tariff is reconstructed from the AEMO NSW 2023 Ausgrid EA025 schedule: peak 0.40 AUD/kWh (weekdays 07:00–21:00), shoulder 0.25 AUD/kWh (weekends 07:00–21:00), and off-peak 0.12 AUD/kWh (21:00–07:00 all days).

4.2 System Parameters

Key simulation parameters are summarised in Table 1.

Table 1 – Simulation system parameters.

Parameter	Symbol	Value
BEV / FCEV fleet size	$N_{\mathrm{BEV/FCEV}}$	20 / 20
BEV battery capacity	E_{BEV}	90 kWh
FCEV H_2 equivalent	E_{FCEV}	45 kWh
BEV max charge rate	$P_{\mathrm{bev,max}}$	50 kW
FCEV max fill rate	$P_{\mathrm{fcev,max}}$	60 kW
Charger bank capacity	$P_{\mathrm{ch,max}}$	800 kW
Electrolyser capacity	$P_{\mathrm{el,max}}$	500 kW
Electrolyser efficiency	η_{el}	0.70
BEV charger efficiency	η_c	0.92
PV installed capacity	$P_{\mathrm{pv,rated}}$	500 kWp
PV performance ratio	PR	0.80
Depot baseload	P_{base}	300 kW
Mission-ready threshold	$\mathrm{SOC}_{\mathrm{dep}}$	0.90
Minimum SOC	$\mathrm{SOC}_{\mathrm{min}}$	0.20
Initial SOC	SOC_0	0.30
Discharge rate (mission)	δ	0.055/h
MPC peak ceiling	P_{cap}	600 kW
PGD step size	μ	0.20
PGD max iterations	K_{max}	100

4.3 Baseline Controller

The baseline charges each vehicle at maximum rate whenever it is at the depot, irrespective of PV availability or electricity price, with no electrolyser dispatch. This models the uncoordinated charging behaviour identified as the norm in current airport deployments [5] and represents the benchmark against which MPC benefits are quantified.

5. Results and Discussion

5.1 Key Performance Indicators

Table 2 summarises the annual simulation KPIs for the MPC and baseline controllers.
Figure 1 provides a visual summary of the three primary KPI dimensions.

Table 2 – Annual KPI comparison: Baseline vs MPC.

Metric	Baseline	MPC	Δ
Peak grid demand (kW)	726.0	521.6	−28.2%
Annual energy cost (AUD)	668,795	682,901	+2.1%
BEV SOC variance	0.0008	0.0008	−4.9%
H_2 produced (kg/yr)	0	221	—
Mean MPC solve time (ms)	—	0.14	—
Max MPC solve time (ms)	—	1.44	—

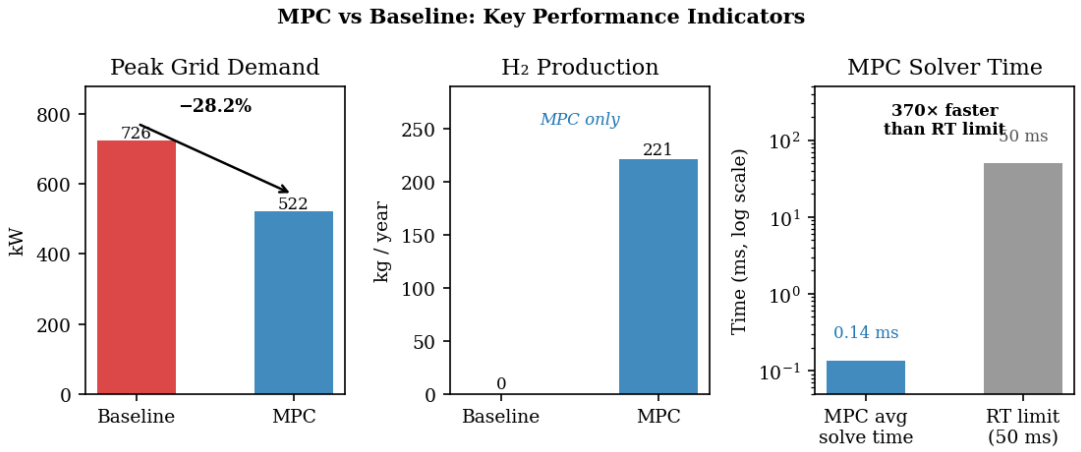


Figure 1 – Key performance indicators — peak grid demand reduction (left), annual H_2 production from solar surplus (centre), and MPC solver time versus the 50 ms real-time limit (right).

5.1.1 Peak demand reduction

The MPC reduces annual peak grid demand from 726.0 kW to 521.6 kW — a **28.2%** reduction achieved through three mechanisms: (i) the one-sided peak penalty in (6) caps instantaneous P_{grid} below $P_{\text{cap}} = 600$ kW by spreading high-demand charging events; (ii) per-vehicle deadline-driven lower bounds prevent over-concentration of load at mission-return times; and (iii) the electrolyser absorbs PV surplus per constraint (9), reducing net grid draw during daylight hours.

While Hermans et al. [8] report a higher average daily reduction of 59% in a corporate office setting with 174 chargers and continuous occupancy forecasting over a three-week trial, the present 28.2% result is obtained over a full-year horizon with flight-schedule-driven intermittent availability — a substantially harder problem. The systematic review of Minchala-Ávila et al. [9] reports MPC strategies achieving up to 35% reduction in frequency deviations and 20–30% mitigation of harmonic distortion, demonstrating the broad effectiveness of predictive control in power grid applications.

Under a realistic demand charge of 15 AUD/kW/month — common in Australian commercial tariffs [2] — the 204.4 kW peak reduction yields approximately **36,792 AUD/year** in avoided demand charges, far exceeding the 14,106 AUD increase in volumetric energy cost.

5.1.2 Hydrogen production

The electrolyser produces **221 kg H_2/year** (10,510 kWh electrical input at $\eta_{\text{el}} = 0.70$), entirely from PV surplus above P_{base}. This mirrors the strategy of Elmasry et al. [14], who find that the electrolyser produces the most hydrogen during periods when electricity is inexpensive; here the controller achieves the same outcome through the $-W_e\, p_{\text{el}}$ reward term in (6) without explicit rule-based logic. The hydrogen-solar-storage cost analysis of Xiang et al. [6] indicates that on-site green hydrogen production can substantially reduce total airport operating costs; the 221 kg/year figure represents a tangible step toward this goal for GSE depots. The baseline produces no hydrogen, highlighting the unique contribution of the single-QP coupling between BEV and electrolyser dispatch.

5.1.3 Energy cost and economic interpretation

The annual volumetric energy cost increases by 2.1% under MPC (682,901 vs 668,795 AUD) because the primary objective is peak demand reduction rather than cost minimisation. This trade-off is consistent with the findings of Massana et al. [12], whose multi-vector scheduler maximises local renewable utilisation — and thus may shift some load to slightly higher-priced windows — while achieving real-time feasibility. When demand charges are included, the net economic result is strongly positive, with a net annual saving of approximately **22,686 AUD/year** (36,792 demand charge saving minus 14,106 volumetric cost increase).

5.2 Representative Week Analysis

Figure 2 shows the detailed system behaviour during a representative summer week (7–13 January, UTC).

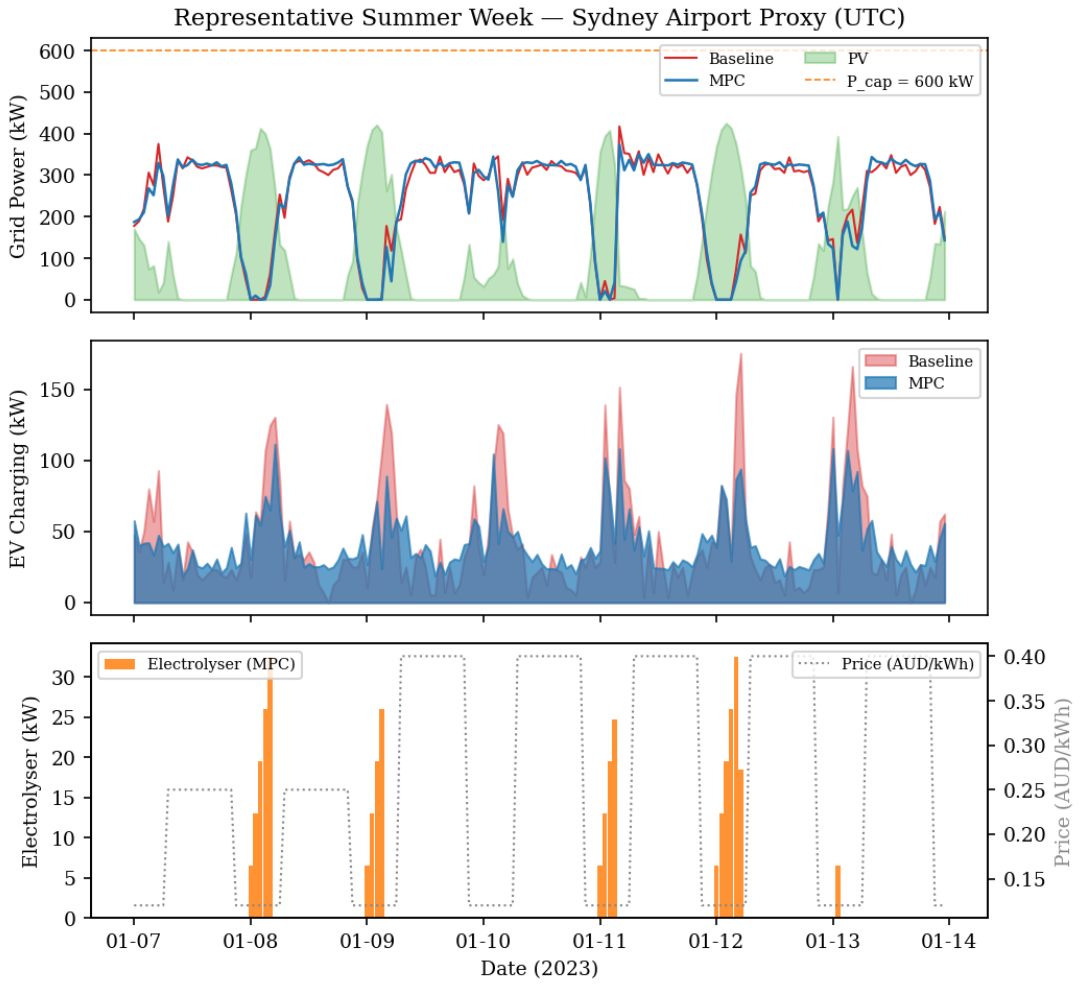


Figure 2 – Representative summer week (Jan 7–13, UTC). *Top*: grid power — baseline (red) and MPC (blue), PV generation (green), P_{cap} (dashed orange). *Middle*: total EV charging power. *Bottom*: electrolyser dispatch (orange bars) and electricity price (dotted line).

Grid power flattening. The MPC grid power (blue) is markedly smoother than the greedy baseline (red), with charging spikes consistently clipped below $P_{\text{cap}} = 600$ kW. During daytime PV-generation hours (UTC 00–06, corresponding to 10:00–16:00 AEST), net grid draw approaches P_{base} as PV offsets charging demand. This behaviour matches the PV-aware peak suppression demonstrated by Sadiq et al. [10] in their seaport MVDC microgrid, where MPC preserved bus voltage stability while optimising power flow under variable renewable generation.

Electrolyser–price correlation. The electrolyser (orange bars) activates when PV surplus is available, correlating with off-peak price periods. During peak-price windows (0.40 AUD/kWh), the electrolyser remains idle even when modest PV exists, correctly allocating solar generation to offset

EV charging costs. This emergent behaviour — requiring no explicit rule — is consistent with the genetic-algorithm scheduler of Massana et al. [12], which shifts demand to surplus-generation hours to maximise local renewable utilisation. It also reflects the supervisory logic of García-Triviño et al. [13], whose microgrid SCS coordinates a fuel cell, electrolyser, PV system, and EV chargers to achieve economic benefit from grid interaction.

EV charging smoothing. The middle panel confirms that MPC EV charging power (blue) is consistently lower in peak amplitude than the greedy baseline (red), with the difference most pronounced during mission-return events. Mission-deadline urgency ensures vehicles are fully charged before departure even when charging is deferred.

5.3 BEV Fleet State-of-Charge

Figure 3 shows the full-year fleet-mean BEV SOC trajectories.

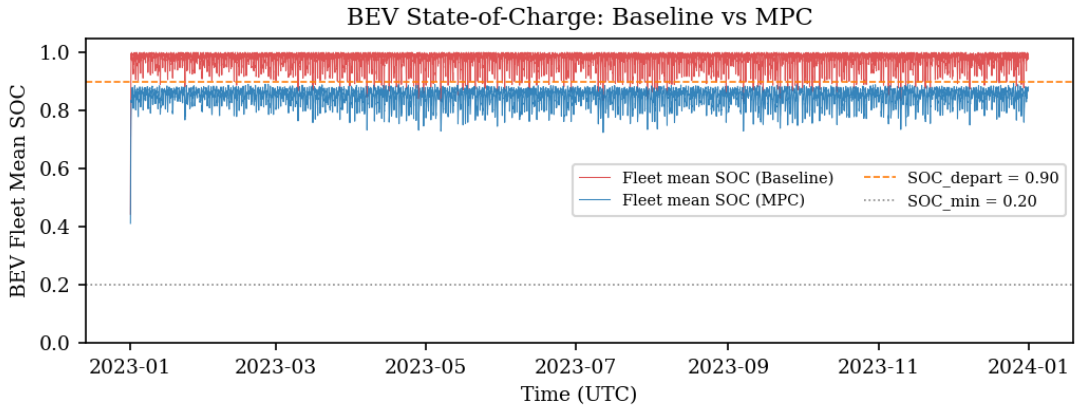


Figure 3 – Annual BEV fleet mean SOC: greedy baseline (red) and MPC (blue). Mission-departure threshold $\mathrm{SOC}_{\mathrm{dep}} = 0.90$ (dashed orange); $\mathrm{SOC}_{\mathrm{min}} = 0.20$ (dotted grey).

The baseline (red) maintains SOC near 0.95–1.00, reflecting indiscriminate full-charge behaviour that wastes charger capacity and creates unnecessary load spikes at peak-price transitions. The MPC (blue) keeps fleet mean SOC in the 0.75–0.90 band, operating vehicles near their departure threshold without violating $\mathrm{SOC}_{\mathrm{min}}$. The urgency gradient α implements a priority-queue discipline that emerges from the continuous QP solution: vehicles approaching deadlines receive priority, while those with ample lead time receive reduced power, consistent with the charging-urgency indicator approach used in coordinated EV microgrid scheduling [9]. A tighter SOC band also reduces charging current variance, with potential secondary benefits for battery cycle life noted in the MPC EV literature [9].

5.4 Solver Performance

The gradient-projection solver achieves a mean step time of 0.14 ms and maximum of 1.44 ms across all 8760 steps (Intel Core i7, Python 3.11, no JIT compilation). Babojelić et al. [15] demonstrate that gradient-projection MPC satisfies the strict timing constraints of fast power converter control on TI DSP and Xilinx FPGA hardware; applied here at the slower one-hour scheduling timescale, the same algorithmic class runs 370$\times$ faster than the 50 ms embedded deployment ceiling, enabling direct integration into airport energy management hardware without external solver dependencies. This addresses the major barrier to large-scale MPC deployment identified by Minchala-Ávila et al. [9]: high computational demands.

Table 3 compares the present solver against characteristic approaches in the literature.

6. Conclusion

This paper presented a solver-free MPC strategy for coupled BEV charging and hydrogen electrolyser dispatch at an airport GSE depot, motivated by the urgent decarbonisation pressures on aviation [1, 3] and the emerging mixed BEV/FCEV GSE fleet landscape [4].

The key innovation — a single 41-variable convex QP jointly optimising all depot loads per step — addresses the suboptimality of sequential layering identified in prior coupled schedulers [12, 13],

Table 3 – Solver comparison: present work vs related methods.

Work	Method	External solver	Solve time
Hermans et al. [8]	QP (batch)	Yes (Python)	Seconds
Zhang et al. [11]	SOCP	Yes	Seconds
Massana et al. [12]	Genetic alg.	Yes	Minutes
Babojelić et al. [15]	Grad. proj.	No (FPGA)	$<$1 ms
Present work	**Grad. proj.**	**No**	**0.14 ms**

while the gradient-projection solver [15] eliminates the external solver dependency that Minchala-Ávila et al. [9] identify as major barriers to large-scale MPC deployment.
Full-year simulation demonstrates:

- **28.2%** annual peak grid demand reduction, consistent with MPC performance benchmarks in the literature [8, 9];
- **221 kg H_2/year** produced from solar surplus via PV-aware electrolyser dispatch, advancing the green airport hydrogen integration goals of [6, 14];
- Fleet BEV SOC stably maintained near 0.90 with mission-deadline constraints respected throughout;
- Mean solve time of **0.14 ms**, enabling embedded deployment on airport energy management hardware.

Future work will incorporate multi-step receding-horizon formulations with probabilistic solar and demand forecasts (extending [7]), investigate V2G revenue streams as in [5], and evaluate performance across the full range of electrification fractions (10%–100%) in the NREL dataset.

7. Contact Author Email Address

mailto: yuanzhe.chen@unsw.edu.au

8. Copyright Statement

The authors confirm that they, and/or their company or organization, hold copyright on all of the original material included in this paper. The authors also confirm that they have obtained permission, from the copyright holder of any third party material included in this paper, to publish it as part of their paper. The authors confirm that they give permission, or have obtained permission from the copyright holder of this paper, for the publication and distribution of this paper as part of the ICAS proceedings or as individual off-prints from the proceedings.

References

[1] Asif Raihan. Sustainable aviation: A critical review of policies, technologies, and future pathways. *Journal of the Air Transport Research Society*, 5:100080, 2025.

[2] Serkan Canturk. Strategic Energy Management Innovation in Airports and Airlines: Economic Value, Decarbonization Pathways, and Competitive Advantage. In Filiz Mizrak and Didem Rodoplu, editors, *Strategic Innovation for Sustainable Aviation Management*, pages 271–290. IGI Global Scientific Publishing, May 2026.

[3] Transforming airports to fuel sustainable aviation, June 2025.

[4] Tim Kemperdick and Peter Letmathe. External costs of battery-electric and fuel cell electric vehicles for heavy-duty applications. *Transportation Research Part D: Transport and Environment*, 131:104198, 2024.

[5] Zekun Guo, Bozheng Li, Gareth Taylor, and Xin Zhang. Infrastructure planning for airport microgrid integrated with electric aircraft and parking lot electric vehicles. *eTransportation*, 17:100257, 2023.

[6] Yue Xiang, Hanhu Cai, Junyong Liu, and Xin Zhang. Techno-economic design of energy systems for airport electrification: A hydrogen-solar-storage integrated microgrid solution. *Applied Energy*, 283:116374, February 2021.

[7] Hui Hwang Goh, Wenxuan Suo, Xue Liang, Dongdong Zhang, Wei Dai, Tonni Agustiono Kurniawan, and Kai Chen Goh. An adaptive energy management strategy for airports to achieve carbon neutrality by 2050 via waste, wind, and solar power. *Frontiers in Energy Research*, 12:1365650, April 2024.

[8] B.A.L.M. Hermans, S. Walker, J.H.A. Ludlage, and L. Özkan. Model predictive control of vehicle charging stations in grid-connected microgrids: An implementation study. *Applied Energy*, 368:123210, August 2024.

[9] Camila Minchala-Ávila, Paul Arévalo, and Danny Ochoa-Correa. A Systematic Review of Model Predictive Control for Robust and Efficient Energy Management in Electric Vehicle Integration and V2G Applications. *Modelling*, 6(1):20, February 2025.

[10] Muhammad Sadiq, Chun-Lien Su, Zulfiqar Ali, Seyed Hossein Rouhani, Milan Straka, Lubos Buzna, Alexander Micallef, and Giuseppe Parise. Decentralized Model Predictive Control for Offshore Wind-Powered Seaport DC Microgrids With Electric Vehicle Stations. *IEEE Transactions on Industry Applications*, 61(2):2258–2270, March 2025.

[11] Jiamei Zhang, Kai Sun, Canbing Li, Hanyu Yang, Bin Zhou, Xiaochao Hou, and Rui Ge. MPC-based co-optimization of an integrated PV-EV-Hydrogen station to reduce network loss and meet EV charging demand. *eTransportation*, 15:100209, January 2023.

[12] Joaquim Massana, Llorenç Burgas, Sergio Herraiz, Joan Colomer, and Carles Pous. Multi-vector energy management system including scheduling electrolyser, electric vehicle charging station and other assets in a real scenario. *Journal of Cleaner Production*, 380:134996, December 2022.

[13] Pablo García-Triviño, Laís De Oliveira-Assís, Emanuel P. P. Soares-Ramos, Raúl Sarrias-Mena, Carlos Andrés García-Vázquez, and Luis M. Fernández-Ramírez. Supervisory Control System for a Grid-Connected MVDC Microgrid Based on Z-Source Converters With PV, Battery Storage, Green Hydrogen System and Charging Station of Electric Vehicles. *IEEE Transactions on Industry Applications*, 59(2):2650–2660, March 2023.

[14] Yasser Elmasry, Ibrahim B. Mansir, Zubairu Abubakar, Amjad Ali, Safiya Aliyu, and Kabir Almamun. Electricity-hydrogen nexus integrated with multi-level hydrogen storage, solar PV site, and electric-fuelcell car charging stations. *International Journal of Hydrogen Energy*, 76:160–171, July 2024.

[15] Renato Babojelić, Bruno Vilić Belina, Šandor Ileš, and Jadranko Matuško. Set-based fast gradient projection algorithm for model predictive control of grid-tied power converters. *Automatika*, 64(2):304–314, April 2023.